



Article

Low-Voltage Capacitor Electrical Discharge Consolidation of Iron Powder

Rosa María Aranda ^{1,*}, Fátima Ternero ² , Beatriz Aranda ¹, Juan Manuel Montes ²  and Francisco G. Cuevas ¹ 

¹ Engineering of Advanced Materials Group, Higher Technical School of Engineering, University of Huelva, Campus El Carmen, Avda. Tres de Marzo s/n, 21071 Huelva, Spain

² Engineering of Advanced Materials Group, Higher Technical School of Engineering, University of Sevilla, Avda. de los Descubrimientos s/n, 41092 Sevilla, Spain

* Correspondence: rosamaria.aranda@dqcm.uhu.es; Tel.: +34-959217448

Abstract: Commercially pure iron powder has been processed by the capacitor electrical discharge consolidation technique. This consolidation technique applies an external pressure and, at the same time, heats a metallic powder mass by the Joule effect of a high-voltage and high-intensity electric current. In this work, a capacitor charged at low voltage has been used instead. The effect of the initial porosity of the Fe powder mass, i.e., of the precompaction pressure, and the number of discharges from the capacitor have been studied. The densification and remaining porosity, the sintering level, the Vickers microhardness, and the electrical resistivity of the sintered compacts have been studied. Compacts sintered by the conventional powder metallurgy route of cold pressing and furnace sintering were also prepared for comparison. Results show that a high initial porosity provides a high electrical resistance in the powder column, a necessary requisite for the Joule effect to increase densification with the number of discharges. Thus, the final porosity decreases to 0.22 after 50 discharges in the powder mass with an initial porosity of 0.30. With this initial porosity, the sintering process increases Vickers microhardness from 29 to 51 HV10 and decreases the electrical resistivity of the powder mass from 3.53×10^{-2} to $5.38 \times 10^{-4} \Omega\cdot\text{m}$. An initial porosity of 0.2 does not make the compacts densify, but a certain bond between particles is attained, increasing microhardness and decreasing electrical resistivity as the number of discharges increases. Lower initial porosities make the powder mass behave as an electrical conductor with no appreciable changes even after 50 electrical discharges.

Keywords: powder metallurgy; FAST; capacitor electrical discharge consolidation; iron powder



Citation: Aranda, R.M.; Ternero, F.; Aranda, B.; Montes, J.M.; Cuevas, F.G. Low-Voltage Capacitor Electrical Discharge Consolidation of Iron Powder. *Metals* **2022**, *12*, 1461. <https://doi.org/10.3390/met12091461>

Academic Editor: Eric Hug

Received: 26 July 2022

Accepted: 28 August 2022

Published: 31 August 2022

Publisher's Note: MDPI stays neutral with regard to jurisdictional claims in published maps and institutional affiliations.



Copyright: © 2022 by the authors. Licensee MDPI, Basel, Switzerland. This article is an open access article distributed under the terms and conditions of the Creative Commons Attribution (CC BY) license (<https://creativecommons.org/licenses/by/4.0/>).

1. Introduction

The production of final parts can be approached in many ways for different types of materials. Powder metallurgy (PM) is a very well-known way [1], working with elemental or alloyed powders and being much extended in metallic materials processing. The conventional and more extended way of PM production consists of pressing powders to obtain a green part (mechanically joined) that is subsequently sintered in a furnace at a temperature under, but near, the melting temperature of the material. The use of a protective atmosphere is generally required to avoid oxidation [2]. In general, the aim of PM production is reducing the porosity to obtain pieces as dense as possible, although at times the presence of a controlled porosity is desirable for final parts, for instance, acting as filters, self-lubricating bearings, biocompatible porous implants, etc. The production of porous materials includes techniques in the vapor state as physical and chemical vapor deposition, in the liquid state as foaming, or in the solid state as the space-holder methods.

Several other varieties of PM processing are highly extended in metallic materials production processes, such as metal injection molding or hot isostatic pressing. Those others related to additive manufacturing have reached their peak in recent years. Moreover, other PM techniques have been studied from many years ago. Thus, the Joule heat generated

by an electric current can be used to sinter powders at the time that pressure is applied to assure both powders contact and lower the electrical resistance. Several different modalities have been conceived and developed for years, all of them with a common characteristic, the quickness of the temperature increase by the Joule effect and the consequent short lasting of the process as compared to the traditional ways. These techniques are indeed referred to in a witted way as FASTs (Field-Assisted Sintering Techniques) [3,4]. Another characteristic of many of these FASTs is the possibility of being carried out in air because these quick processes do not generate oxidation problems.

Among the FASTs, maybe the most extended one is Spark Plasma Sintering (SPS) [5], which is characterized by using a conductive die. The heat is thus transferred to the material to be sintered in an indirect and relatively slow way. Some other FASTs are specifically applied to metallic materials because the electric current directly flows through the powder mass, making, in this case, necessary the use of an insulating die of ceramic nature to avoid current drifts. The applied pressure is usually limited because of the mechanical strength of the highly conductive and ductile Cu-based electrodes and of the ceramic die. The first developed FAST is known as Electrical Resistance Sintering (ERS) [6,7]. The ERS process is mainly controlled by selecting a high-intensity current, as well as the current passing time (usually in the order of the second). The attained voltage will depend on the electrical resistance of the powder column in each moment of the process. A practical way to implement this technique is through the use of a spot-welding machine [8], which conveniently adapted can fit the process requirements.

A FAST with higher power can be required for powders that are difficult to sinter, for instance, because of the presence of persistent oxide layers surrounding powder particles or when the time at high temperature must be minimized to preserve a certain microstructure. An option to consider in these cases is to store energy in a capacitor that can be quickly discharged (in the order of the millisecond), at the time that the powders are pressed [9]. This technique is known as capacitor electrical discharge consolidation (CEDC), developed during the end of the 1970s and beginning of the 1980s [10,11]. The stored energy is controlled by the capacity and the charge voltage with a linear and a square dependence on these two parameters, respectively.

CEDC usually requires the application of an external pressure to help consolidation. When pressure is lower than a certain required value, the electrical resistance of the powder mass can exceed the limit to allow the current to pass through with enough intensity to get an appropriate consolidation. Under these circumstances of low-energy input, the current could not overcome the air gaps between particles, producing intense sparking and resulting in the rupture of the surrounding die [12]. Furthermore, local conductive channels or paths could appear in the powder column, which absorb the whole energy creating inhomogeneous structures. On the other hand, when enough pressure is applied, the friction between particles forces the descaling of the dielectric oxide layers that normally cover the metallic powder particles [13] and very much affects the resistivity of the powder column [14,15]. Additionally, when capacitors are charged at high voltages, the sudden potential difference can homogeneously break and clear the oxide films by an electrical explosion at particle contacts [16,17]. Conversely, excessive pressures could make interparticle contacts reach a low temperature, insufficient to destroy the particle surface oxide films, affecting the consolidation of the sample [17,18]. Under appropriate conditions, the temperature reached in the powder particle contacts can be very high. Estimations based on the specific heat of the powder and the input power, calculated by integrating the current and voltage during the discharge, point out values as high as 1058 and 4925 °C for Ti and Ti-6Al-4V powder particles processed with 450 μ F and up to 2.86 kJ/g [19,20], or about half of those values for Ti-6Al-4V powder under the processing conditions of 240 μ F and 0.5 to 2.5 kJ/g [21]. Temperatures of up to 2593 to 6193 °C are reported in mixed Ti-Al25 powder processed with 450 μ F and 1.67 to 5 kJ/g [22] or of up to 2004 to 5038 °C in mixed Ti-Si37.5 powder processed with 300 μ F and 7.35 to 15.29 kJ/g [23].

Nevertheless, consolidation is also possible in the absence of external pressures for remarkable intensity of the current passing through the powder aggregate. Under these circumstances, the action of internal electromagnetic pressures [16], due to the pinch effect (the magnetic field generated when an axial current circulates through a long cylindrical metal powder column, which tends to contract the column radially), should be considered. Estimated values in the powder column center were, for instance, up to 522 MPa for an energy input of 2.5 kJ/g and Ti–6Al–4V powder (stacked in a linear manner) in a 3.3 mm in diameter column [21] or even much higher pressures of up to 2900 MPa for Ti–Si37.5 powder stacked in a linear manner when processed with 15.29 kJ/g [23].

In practice, appropriate conditions are reached by using custom high-voltage equipment. Thus, some examples can be mentioned, as the use of up to 6 kV and 1800 μF to reach a maximum energy of 32 kJ applied to Ti, Nb, and Ta powders [24]; the use of a capacitor bank of 450 μF and 6 kV to reach up to 8 kJ in a Ti–Si alloy [25]; 360 μF and 6.5 kV to reach up to 7.5 kJ in a WC–10Co-cemented carbide [26]; 6000 μF capacitors charged at 6 kV in WC–Co powder processed with 108 kJ [27]; 32 kJ reached at 6 kV on Fe powder [18]; 80 μF at 13.5 kV in steel, Fe, Ni, and Cu powders [28]. Some other examples are detailed in [9], among them, a special mention is deserved of those carried out with iron or iron-based materials, as experimented in this paper. Pure iron is well-known in conventional sintering, and development studies of CEDC were carried out with iron [10,29], moreover, it has also been used more recently, both with as-received [17,18,28,30,31] and mechanically ground [32] powder. Plain carbon steel was processed by CEDC also in the initial steps of this technique [33,34]. More recently, porous stainless steel filters [35], wear-resistant cold-worked steel [36], AISI M2 high-speed steels [30], Fe–Cr–Mo steel [37], heat-resistant steel [17], 13Cr–2Mo oxide dispersion strengthened (ODS)-steel [38], pipeline steel [39], M84 steel [28,40], mixtures as Fe-based-TiC (Ferro-Titanit Nikro128) powders [41], Fe–diamond [42], Fe–20TiC mixed with diamond powder [43], or Fe–20Ti–5B4C powders [44] have been consolidated with this technique. A different research interest was, moreover, considered in early studies [45], where Fe–9Si–13B amorphous soft magnetic alloys were consolidated trying to preserve the amorphous state with this quick process. The influence of the process on the microstructure was studied with mechanically alloyed Fe–1.5Mo [46] or AISI M2 powders [47]. The subjacent idea on all these experiments was to increase the store energy by using high-voltage equipment, which can also help to force the appearance of electric paths in the powder mass; therefore, improving sintering. High voltages require dedicated equipment that are not completely based on solid state physics devices, with relatively high prices.

Nevertheless, low-voltage experiments have been at times carried out; in this case, with relatively high capacitance. For instance, 50 V and 3840 μF were applied to Fe–TiC to recycle the expensive chips of machined annealed Ferro-Titanit, obtaining bulk pieces consisting of TiC with a size of approximately 2 μm and hardness like the original material [41]. Applied to mixtures of steel powders of different compositions were 24 V and 7500 μF , resulting in a microstructure denser than 99%, but with fracture surfaces showing weak adhesions between the powder particles of dissimilar powders [36]. Finally, 270–400 V and 25000 μF were applied to Ti, or a low-melting temperature material, such as Sn [12]. Ti was processed after being pressed at 710 MPa (relative density of about 80%) to reach a 90% relative density. The density of Sn increased from 7.2 g/cm^3 after pressing to 7.3 g/cm^3 after discharging, with no individual particles found in the microstructures after consolidation.

In this paper, we will experiment with low voltages, but very high capacities, using a small and cheap piece of commercial equipment adapted from a stud welder [48]. Having a relatively low energy, several cycles will be applied to check the effect on Fe powder. The main interest of this study is to understand the mechanisms of sintering in low-voltage capacitor discharge conditions.

The attained densification in the compact, the hardness, and the resulting resistivity after consolidation will be studied for a different number of discharges. In general, this

technique will allow for the obtaining of a consolidated porous material. The results obtained will be compared with those of compacts consolidated by the conventional PM route of cold pressing and vacuum furnace sintering.

2. Materials and Methods

The only need regarding the equipment to carry out the CEDC process is a capacitor or a group of capacitors (a bank) with the appropriate electrical conditions, which is adequately fulfilled with stud welding equipment. In this work, the typical welding gun of these equipment has only maintained the switching function, being in practice substituted by Cu electrodes (99.9% Cu–0.04% O) and thermal wafers (99.06% Cu, 0.760% Cr, 0.08% Zr, and 0.035% Ni), regarding the electric current conduction. Electrodes also act as punches to press the powder particles. The stud welding machine Nomark 10S (Thomas Welding, Jumet, Belgium) with a capacity of 132,000 μF and a charging voltage of 200 V has been used. These values allow for the storing of a maximum energy of 2640 J. Moreover, the consolidation assembly consisted of a thick 40 mm in diameter sialon die with an inner orifice of 8 mm in diameter, which is closed by the Cu electrodes and wafers, with the required diameter to avoid any leak of the powder placed between them during consolidation (Figure 1).

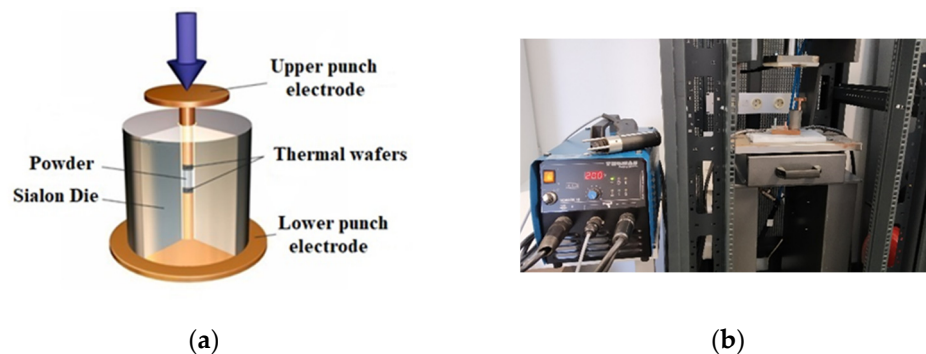


Figure 1. (a) Scheme of the sintering assembly, including electrodes and die, used in the CEDC experiments. (b) Stud welding equipment and pneumatic press used in the experiments.

The working sequence before the CEDC process consisted of pouring 1 g of Fe powder (Atomet 1001HP, Rio Tinto Metal Powders, Canada), as shown in Figure 2, into an 8-millimeter internal diameter wall-lubricated steel die. This 99.4% purity (main impurities being 0.09% Mn, 0.06% O, 0.005% S, and 0.004% C) atomized powder with mean particle size $D[4,3] = 162 \mu\text{m}$ was then vibrated until the powder particles reached their tap density [49] of 2.9 g/cm^3 (porosity of 0.63 ± 0.05). This assures a common starting situation in the different experiments. The powder mass was then pressed at 200, 400, or 1000 MPa in a universal testing machine to obtain green compacts with initial porosities of 0.3, 0.2, or 0.1.

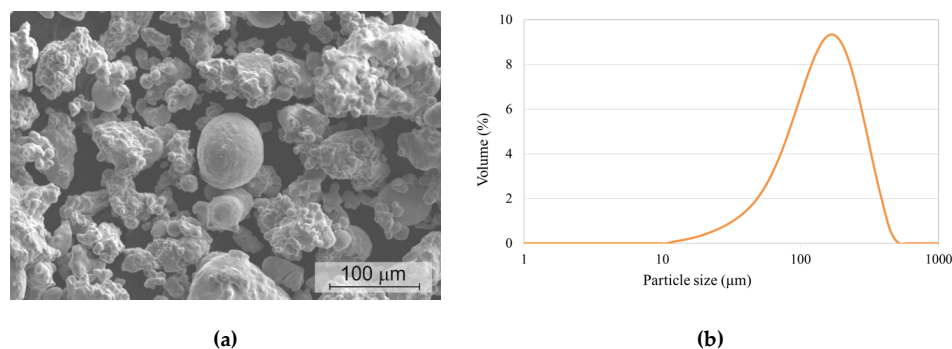


Figure 2. (a) SEM micrograph and (b) granulometric distribution of the Fe Atomet 1001HP powder used in the CEDC experiments.

These compacts were then placed into a previously graphite-lubricated (deposited through an acetone suspension) sialon die to carry out the CEDC process. A pressure of 200 MPa was applied by a pneumatic press, for all the green compacts, to ensure good contact between electrodes and compact during the discharge process. The capacitor was then charged and discharged the required number of times, with an interval of 5 s between two discharges. The number of discharges increased by 5 until it reached a maximum of 50. The number of discharges can easily be translated to the total applied energy by knowing that one discharge corresponds to 2.64 kJ. Four compacts for each configuration were prepared to measure the different properties and to calculate mean values.

Four 1 g–8 mm in diameter compacts were also conventionally consolidated, i.e., cold-compacted at 500 MPa (die wall lubrication) and vacuum furnace-sintered at 1175 °C (heating at 20 °C/min up to 1075 °C, at 10 °C/min up to 1125 °C, at 5 °C/min up to 1170 °C, and then at 1 °C/min up to the sintering temperature) for 30 min (cooling was carried out by switching off the heating system). The final porosity of these compacts was about 0.15 ± 0.01 , an adequate value to be compared with the CDEC compacts (porosities under 0.08–0.09 can be reached with conventional processing by using reducing atmospheres with specially designed Fe powder [50,51]).

All the electrical-sintered and furnace-sintered compacts were analyzed to determine the final porosity, the sintering level, the microhardness, and the electrical resistivity. The porosity of the compacts was determined by weighing and measuring the specimen and by the Archimedes' method [52]. The final porosity (Epiphot 200, Nikon, Tokyo, Japan) and the HV10 Vickers microhardness [53] (DuraScan 50G5, Emcotest, Kuchl, Austria) were studied on diametrical sections of resin-embedded compacts. Microhardness values were measured at the compact center and each of the quadrant centers, and mean values and standard deviations were calculated for each one of the compacts. The sintering level was studied on mechanically broken surfaces (after holding half compact and a sudden impact on the other half) by scanning electron microscopy, SEM (JSM-IT500HR, Jeol, Tokyo, Japan). A four-points probe and a Kelvin bridge (CA 10, Chauvin Arnoux, Paris, France) were used for the electrical resistance measurements at room temperature, with a measuring range between 0.01 mΩ and 1000 Ω and values in the range 0.1–9850 mΩ. The thermoelectric effects were eliminated by changing the probes polarity in two different measurements, and the mean value was considered for each specimen. For the probe electrodes spacing ($d = 1$ mm), the electrical resistivity of the material can be calculated as indicated in Equation (1) [54]:

$$\rho = 2\pi d R_{measured} \quad (1)$$

The relative error in the resistivity calculation, according to the uncertainty in the measurement of the resistance values, is always lower than 7%.

3. Results and Discussion

3.1. Densification Evolution

The final porosity Θ of the CEDC compacts, according to the Archimedes' values, as a function of the initial porosity and the number of discharge cycles n (i.e., the applied energy), is given in Figure 3. Results obtained from the compacts measurement and weight give porosity values slightly higher, with the same trend. For both methods, a deviation lower than 0.03 is obtained from the measurements of similar specimens.

As shown, the final porosity is affected by the precompaction pressure and, only for the powder mass with an initial porosity of 0.3, by the number of discharge cycles. For an initial porosity of 0.3, a high electrical resistance is maintained in the powder mass, and the heat generated by the current passage under the applied pressure of 200 MPa makes the powder column densify. A significant decrease in porosity of about 30% is observed, reaching a value of 0.215 after 50 discharges. It was checked that a higher number of discharges did not improve the densification of the specimens.

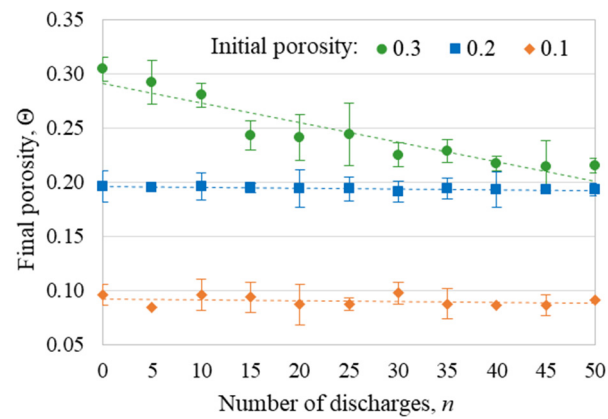


Figure 3. Final porosity of the compacts (Θ) versus the number of discharges, as measured by the Archimedes' method.

Starting from lower porosities makes the CEDC process have little influence on the final porosity of the specimens. Nevertheless, it is known that high temperatures of up to 103–104 °C can be attained in the contacts between powder particles, and it should be checked whether particles have bonded to each other under these initial conditions.

3.2. Densification Evolution

Figure 4 shows the porosity distribution in the green compacts and after 50 discharges for the different initial porosities.

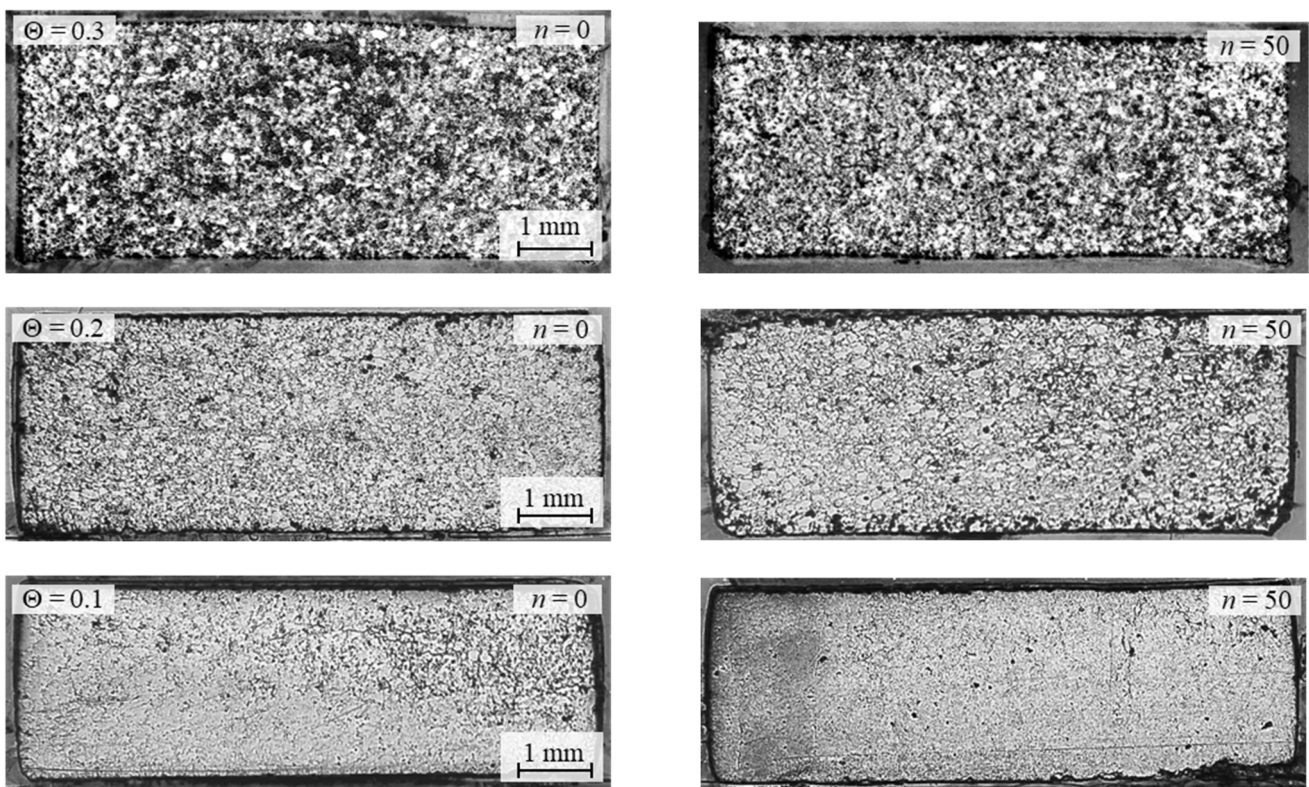


Figure 4. Optical macrographs showing the porosity distribution of the CEDC specimens after 0 and 50 discharges.

As observed in Figure 4, the porosity of the $\Theta = 0.3$ specimen decreases after 50 discharges, whereas for the other initial porosities, it does not appreciably change. Regarding the porosity distribution, Figure 4 shows that, as a priori desirable, there is little difference

between the specimen center and periphery because the quick CEDC process does not heat in excess the powder particles, but only their contacts, obtaining a porosity distribution like that obtained after the precompaction process. Nevertheless, the typical heterogeneity appearing in die compacting processes [55] should always be considered. A slower FAST process, such as ERS, with the whole energy applied in only one current passing event results in more heterogeneous microstructures, even making it possible to reach a totally densified center and a very porous periphery because of the Joule heat concentration in the center and the heat leaks through the die and electrodes [56]. However, when the process is much slower and diffusion processes have the necessary time to eliminate gradients, as happening in other FAST processes, such as spark plasma sintering [57], the microstructure is also very homogeneous.

Details of the porosity evolution with the number of discharges can be observed in Figure 5 (the porosity distribution for the conventionally sintered specimen is also shown). For the CEDC specimens, the densification and particles bonding for a high initial porosity can be appreciated. However, for a low initial porosity, the process is little effective because the powder mass behaves as a good electrical conductor and very low Joule heat is generated. Interparticle boundaries can be easily appreciated in this situation even after 50 discharges. Regarding the furnace-sintered specimen, and according to its porosity, it should be placed between the specimens with $\Theta = 0.2$ and $\Theta = 0.1$ after 50 discharges. As observed in Figure 5b, the porosity is probably more homogeneously distributed, and pores seem to have evolved to more rounded shapes, as expected from a sintering process lasting enough time for diffusion processes to take place. Moreover, the limits of interparticles completely disappear in micrographs.

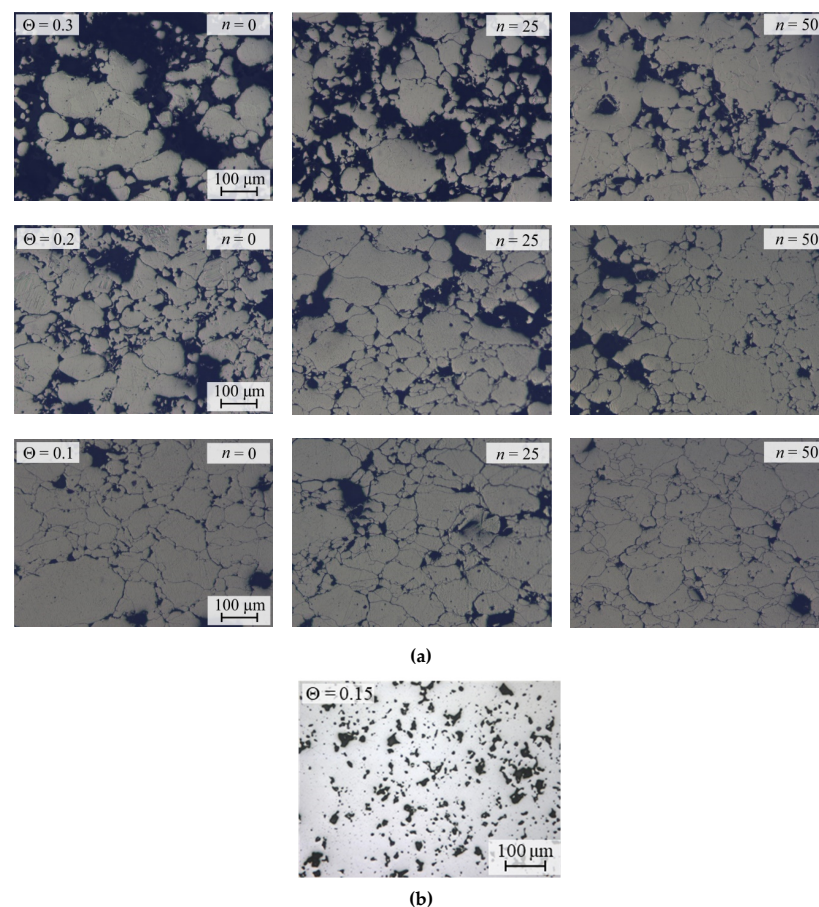


Figure 5. Micrographs showing the porosity distribution for (a) different discharges of the specimen with initial porosities of 0.3, 0.2, and 0.1, and (b) the conventionally sintered compact.

The fracture surfaces of mechanically broken specimens were studied to observe the bonds or necks between particles after the discharges. Figure 6 shows the fracture surface after a different number of discharge cycles in the specimens with an initial porosity of 0.3, 0.2, and 0.1. For $\Theta = 0.3$ and after five discharges, weak bonds start to appear between particles, being easily broken. Necks seem to get more and more stable with the number of discharges, up to form good bonds revealed by the appearance of features characteristic of a ductile behavior, as shown for 30 discharges. In addition, the high temperature reached in some contacts seem to reveal the melting and quenching generated by the Joule heat, observing a colony of microparticles adhered to the surface, as described for tungsten powder in [58]. Therefore, for an initial high porosity, the powder column has a high electrical resistance, generating enough energy by Joule effect for the consolidation process and densifying the powder mass.

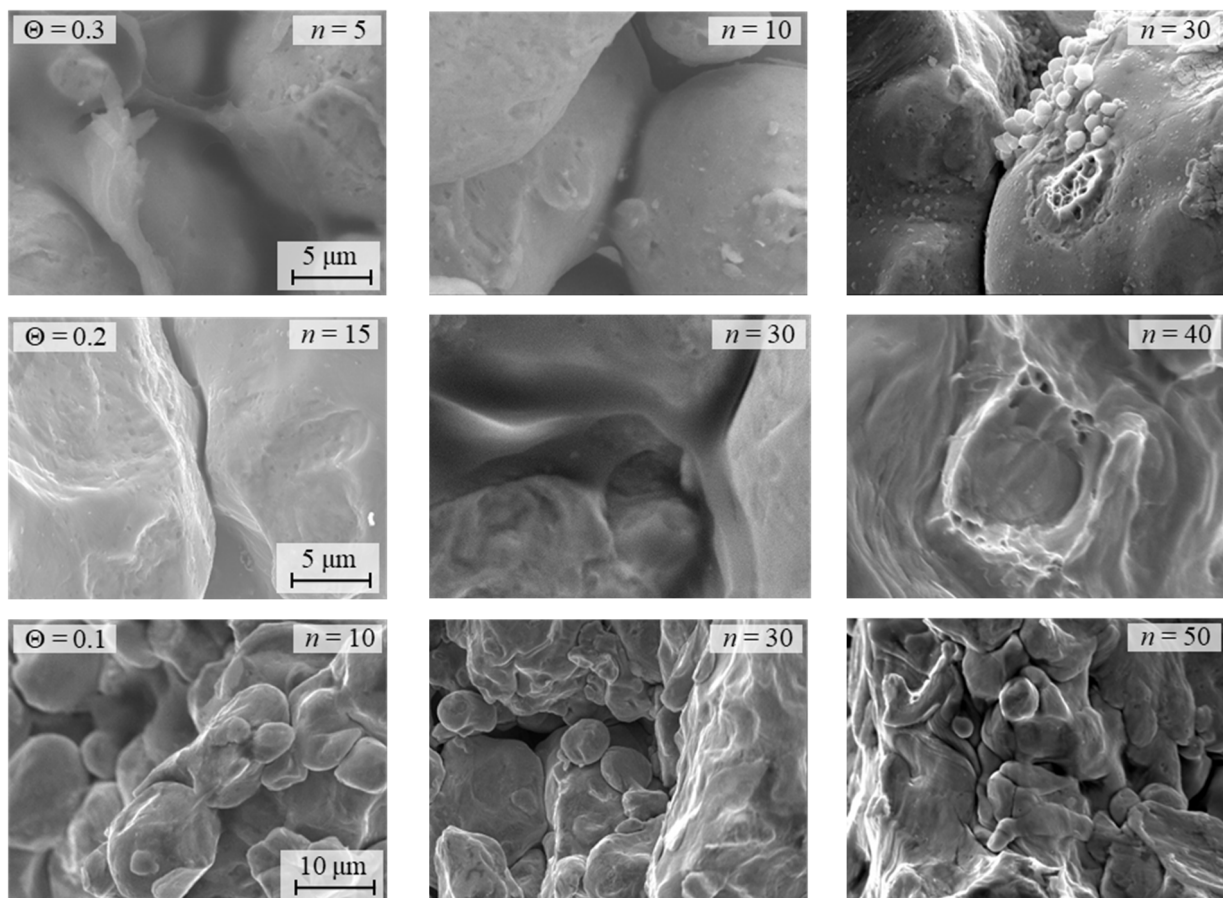


Figure 6. Fracture surface of the specimens with initial porosity of 0.3, 0.2, and 0.1 after the number of discharges indicated at each image.

A similar evolution can be observed in the specimens with an initial porosity of 0.2, with the appearance of necks between particles and the features of ductile fracture after several discharges. Despite this, the final porosity does not decrease, as previously explained.

In contrast, in the specimens with an initial porosity of 0.1, changes are not observed in the fracture with the number of discharge cycles. Powder particles appear deformed because of the external pressure, but no bonds between particles nor signs of ductile fracture are observed. Probably, the precompaction pressure makes the powder particles have numerous and good quality metal–metal contacts, making the material behave as a current conductor with a low Joule effect.

3.3. Microhardness Evolution

The microhardness of the compacts, for the different initial porosities, is represented versus the number of discharges and the final porosity in Figure 7.

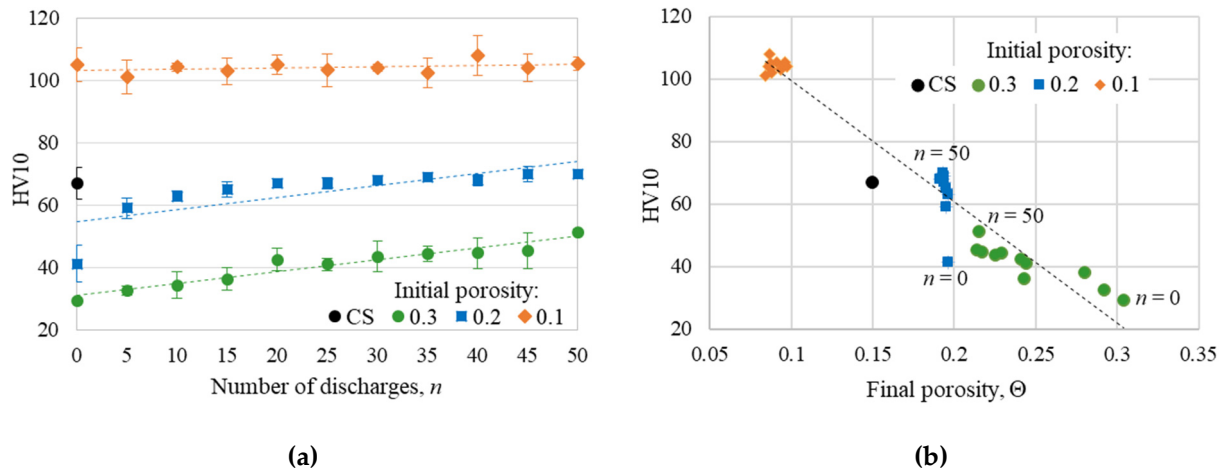


Figure 7. Microhardness (HV10) of the CEDC specimens with initial porosities of 0.3, 0.2, and 0.1 as a function of (a) the number of discharges and (b) the final porosity. Microhardness of the conventionally sintered (CS) specimen is given for comparison.

As expected, Figure 7 shows that microhardness increases with the decrease in the initial porosity, changing from about 29 to 105 HV10. Moreover, the number of discharges affects the microhardness for initial porosities of 0.3 and 0.2. This agrees with the results regarding the formation of bonds between particles. For a lower initial porosity of 0.1, all the microhardness values are inside the experimental uncertainty, not forming bonds between particles because of the low heat generated in the particle contacts.

A linear trend between microhardness and final porosity is shown in Figure 7b, with values ranging from 29 to 109 HV10. It also shows the influence of the number of discharges, affecting both the final porosity and the microhardness for an initial porosity of 0.3, only affecting the microhardness for an initial porosity of 0.2, and not showing any influence for an initial porosity of 0.1, with values grouped inside the standard deviation.

Also shown in Figure 7, the microhardness of the conventionally processed specimen, pressed at 500 MPa, results in 67 HV10, in the order of that of specimens compacted at a lower pressure of 400 MPa ($\Theta = 0.2$) and electrically processed, despite the processing time at a high temperature being much shorter for these. The high temperature achieved in the particles' contact with the CEDC process and the elimination of the oxide layer surrounding the powder particles can be the cause of this difference, taking also into account that furnace sintering is, probably, not completely effective to achieve an adequate bonding when taking place in a non-reducing atmosphere.

3.4. Electrical Resistivity Evolution

An alternative way to check the effect of the electrical consolidation on the sintering level is through the measurement of the electrical resistivity of the specimens. Figure 8 shows the measured values represented versus the number of discharges and the final porosity.

As shown, the resistivity decreases with a decreasing initial porosity and an increasing number of discharges because of the decrease in porosity and better contacts between particles. Again, the effect of the electrical discharges is clear for 0.3 and 0.2, but not for a lower initial porosity of 0.1.

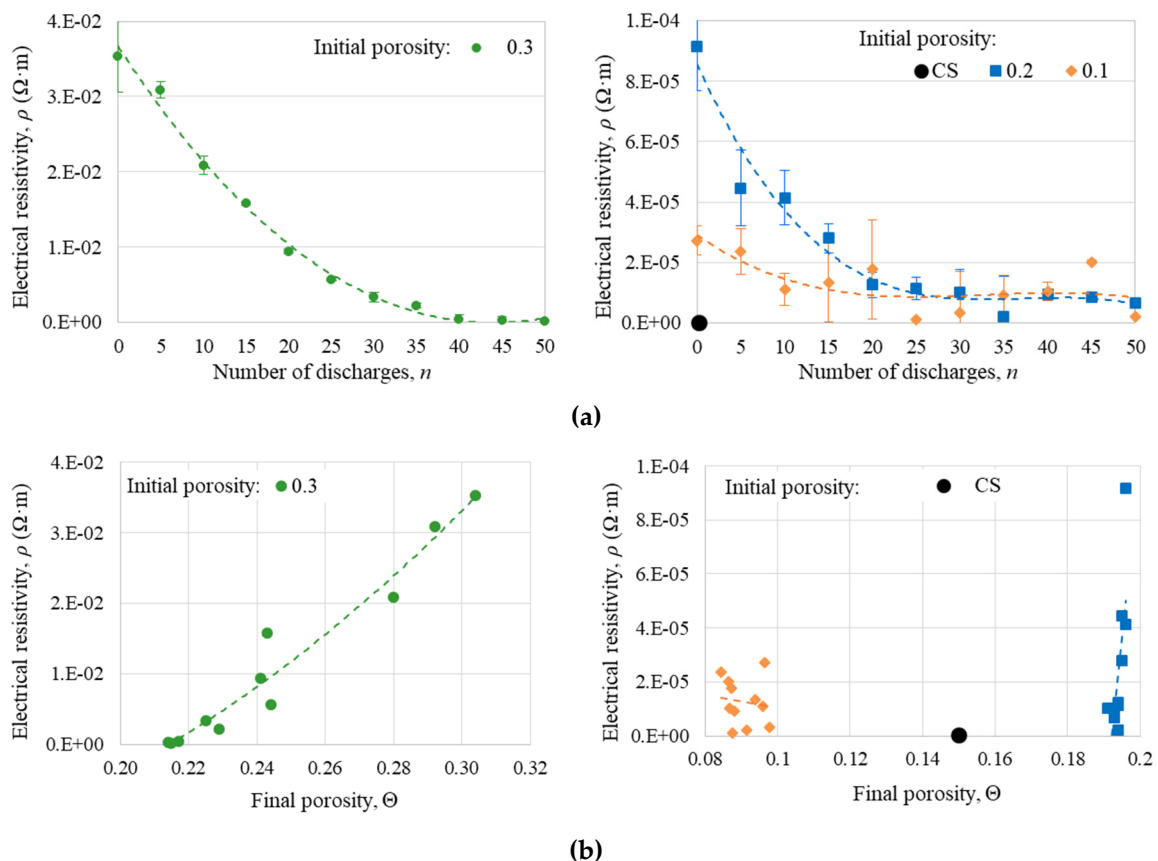


Figure 8. Electrical resistivity for the different CDEC compacts vs. (a) number of discharge and (b) final porosity. The value for the conventionally sintered specimen (CS) is also shown.

Comparing the values obtained for the samples consolidated by CDEC and that obtained by conventional sintering, the latter has a resistivity almost one order of magnitude lower. The time at a high temperature during conventional sintering allows the formation of easy ways for the current to pass; therefore, decreasing the value of the resistivity.

4. Conclusions

A commercially pure Fe powder has been consolidated by the CEDC process with initial porosities of 0.3, 0.2, and 0.1, and the application of between 0 and 50 discharges.

It has been proven that this technique can be applied to consolidate powder columns with commercial equipment adapted from the stud welding technology and only charging the capacitor at 200 V. However, when comparing it with the studies in the bibliography included in the Introduction section, the results are far from those obtained with specifically designed high-voltage equipment, with only one discharge being necessary to consolidate the powder column and making it possible to attain a higher densification when a relatively high pressure is applied at the time that the electric current circulates through the powder column.

To obtain a clear change in densification and bond between the powder particles, a high resistivity is required so that the current generates enough Joule heat in the powder particles' contacts. Thus, after 50 discharges, porosity can decrease from 0.3 to 0.2 with a hardness increase from 29 to 51 HV10 and a decrease in the electrical resistivity from 3.53×10^{-2} to $1.44 \times 10^{-4} \Omega \cdot m$. With an initial porosity of 0.2, the process does not make the powder mass densify, but powder particles are better joined after several discharges. For an initial porosity of 0.1, the electric current does not have an appreciable effect on the powder mass.

With this technique, porous materials with the desired final porosity in the range of 0.15 to 0.3 and an adequate level of sintering between the powder particles could be obtained by changing the processing conditions. There is no need to use high-temperature furnaces or sintering atmospheres, and the very quick process should ensure the preservation of the original microstructure of the original powder.

Author Contributions: Conceptualization, F.G.C. and J.M.M.; methodology, R.M.A. and F.T.; validation, R.M.A. and B.A.; writing—original draft preparation, R.M.A.; writing—review and editing, F.G.C. All authors have read and agreed to the published version of the manuscript.

Funding: This research was funded by Junta de Andalucía, grant to the Research Group TEP-971 and the University of Seville Research Funding Program, grant number 2020/00000647.

Data Availability Statement: Not applicable.

Conflicts of Interest: The authors declare no conflict of interest. The funders had no role in the design of the study; in the collection, analyses, or interpretation of data; in the writing of the manuscript; in the decision to publish the results.

References

1. Tan, Z.-Q.; Zhang, Q.; Guo, X.-Y.; Zhao, W.-J.; Zhou, C.-S.; Liu, Y. New development of powder metallurgy in automotive industry. *J. Cent. South Univ.* **2020**, *27*, 1611–1623. [[CrossRef](#)]
2. Tan, Z.-Q.; Engström, U.; Li, K.; Liu, Y. Effect of furnace atmosphere on sintering process of chromium-containing steel via powder metallurgy. *J. Iron Steel Res. Int.* **2021**, *28*, 889–900. [[CrossRef](#)]
3. Olevsky, E.A.; Dudina, D.V. *Field-Assisted Sintering: Science and Applications*; Springer Nature: Cham, Switzerland, 2018; pp. 1–425.
4. Weston, N.S.; Thomas, B.; Jackson, M. Processing metal powders via field assisted sintering technology (FAST): A critical review. *Mater. Sci. Technol.* **2019**, *35*, 1306–1328. [[CrossRef](#)]
5. Salvetr, P.; Dlouhý, J.; Školáková, A.; Průša, F.; Novák, P.; Karlík, M.; Haušild, P. Influence of Heat Treatment on Microstructure and Properties of NiTi46 Alloy Consolidated by Spark Plasma Sintering. *Materials* **2019**, *12*, 4075. [[CrossRef](#)]
6. Taylor, G.F. Apparatus for Making Hard Metal Compositions. U.S. Patent 1,896,854, 7 February 1933.
7. Lenel, F.V. Resistance sintering under pressure. *JOM* **1955**, *7*, 158–167. [[CrossRef](#)]
8. Montes, J.M.; Cuevas, F.G.; Ternero, F.; Astacio, R.; Caballero, E.S.; Cintas, J. Medium-frequency electrical resistance sintering of oxidized C.P. iron powder. *Metals* **2018**, *8*, 426. [[CrossRef](#)]
9. Aranda, R.M.; Ternero, F.; Lozano-Pérez, S.; Montes, J.M.; Cuevas, F.G. Capacitor electrical discharge consolidation of metallic powders—A review. *Metals* **2021**, *11*, 616. [[CrossRef](#)]
10. Clyens, S.; Al-Hassani, S.T.S.; Johnson, W. The compaction of powder metallurgy bars using high voltage electrical discharges. *Int. J. Mech. Sci.* **1976**, *18*, 37–40. [[CrossRef](#)]
11. Alp, T.; Al-Hassani, S.T.S.; Johnson, W. The electrical discharge compaction of powder: Mechanics and material structure. *J. Eng. Mater. Technol. Trans. ASME* **1985**, *107*, 186–194. [[CrossRef](#)]
12. Rajagopalan, P.K.; Desai, S.V.; Kalghatgi, R.S.; Krishnan, T.S.; Bose, D.K. Studies on the electric discharge compaction of metal powders. *Mater. Sci. Eng. A* **2000**, *280*, 289–293. [[CrossRef](#)]
13. Evans, U.R. *The Corrosion and Oxidation of Metals: First Supplementary Volume*; Edward Arnold: London, UK, 1968.
14. Montes, J.M.; Cuevas, F.G.; Cintas, J.; Gallardo, J.M. Electrical conductivity of metal powder aggregates and sintered compacts. *J. Mater. Sci.* **2016**, *51*, 822–835. [[CrossRef](#)]
15. Montes, J.M.; Cuevas, F.G.; Cintas, J. Electrical resistivity of a titanium powder mass. *Granul. Matter* **2011**, *13*, 439–446. [[CrossRef](#)]
16. Kim, D.K.; Pak, H.R.; Okazaki, K. Electrodischarge Compaction of Nickel Powders. *Mater. Sci. Eng. A* **1988**, *104*, 191–200. [[CrossRef](#)]
17. Grigoryev, E.G.; Olevsky, E.A. Thermal processes during high-voltage electric discharge consolidation of powder materials. *Scr. Mater.* **2012**, *66*, 662–665. [[CrossRef](#)]
18. Grigoryev, E.G.; Olevsky, E.A.; Yudin, A.V.; Yurlova, M.S. Wave mode high voltage consolidation of powder materials. *Comput. Mater. Sci.* **2015**, *100*, 8–14. [[CrossRef](#)]
19. Jo, Y.H.; Kim, Y.H.; Jo, Y.J.; Seong, J.G.; Chang, S.Y.; Reucroft, P.J.; Kim, S.B.; Lee, W.H. Self-Consolidation Mechanism of Porous-Surfaced Ti Implant Compacts Induced by Electro-Discharge-Sintering of Spherical Ti Powders. *Met. Mater. Int.* **2015**, *21*, 337–344. [[CrossRef](#)]
20. Lee, W.H.; Jo, Y.J.; Kim, Y.H.; Jo, Y.H.; Seong, J.G.; Van Tyne, C.J.; Chang, S.Y. Self-consolidation mechanism of porous Ti-6Al-4V implant prototypes produced by electro-discharge-sintering of spherical Ti-6Al-4V powders. *Arch. Metall. Mater.* **2015**, *60*, 1185–1189. [[CrossRef](#)]
21. Lee, W.H.; Puleo, D.A. Mechanism of consolidation of a porous-surfaced Ti-6Al-4V implant formed by electrodischarge compaction. *J. Mater. Sci. Lett.* **1999**, *18*, 817–818. [[CrossRef](#)]

22. Jang, H.; Cho, Y.; Kang, T.; Kim, K.; Lee, W. A Study on the Synthesis and Consolidation of Ti3Al by Electro-Discharge. *J. Kor. Inst. Met. Mater.* **2009**, *47*, 488–493.
23. Chang, S.Y.; Cheon, Y.W.; Yoon, Y.H.; Kim, Y.H.; Kim, J.Y.; Lee, Y.K.; Lee, W.H. Self-consolidation mechanism of Ti5Si3 compact obtained by electro-discharge-sintering directly from physically blended Ti-37.5 at.% Si powder mixture. *Arch. Met. Mater.* **2017**, *62*, 1299–1302. [[CrossRef](#)]
24. Dzmityry, M.; Klimenty, B. A porous materials production with an electric discharge sintering. *Int. J. Refract. Met. Hard Mater.* **2016**, *59*, 67–77. [[CrossRef](#)]
25. Cheon, Y.W.; Jo, Y.J.; Lee, C.M.; Jang, H.S.; Kim, K.B.; Lee, W.H. Consolidation of mechanical alloyed Ti–37.5 at.% Si powder mixture using an electro-discharge technique. *Mater. Sci. Eng. A* **2007**, *467*, 89–92. [[CrossRef](#)]
26. Wu, X.Y.; Zhang, W.; Wang, W.; Yang, F.; Min, J.Y.; Wang, B.Q.; Guo, J.D. Ultrafine WC-10Co cemented carbides fabricated by electric-discharge compaction. *J. Mater. Res.* **2004**, *19*, 2240–2244. [[CrossRef](#)]
27. Grigoryev, E. Chapter 17. High Voltage Electric Discharge Consolidation of Tungsten Carbide—Cobalt Powder. In *Nano-Composites with Unique Properties and Applications in Medicine and Industry*; Cuppoletti, J., Ed.; IntechOpen Limited: London, UK, 2011; pp. 345–360.
28. Darvizeh, A.; Alitavoli, M.; Namazi, N. On the effects of circuit parameters on electrical behaviour of metallic powders subjected to high rate discharge compaction process. *Powder Metall.* **2020**, *63*, 94–103. [[CrossRef](#)]
29. Williams, D.J.; Johnson, W. Heat generation in the high voltage discharge forming of sponge iron powders. In Proceedings of the Twenty-First International Machine Tool Design and Research Conference, Swansea, UK, 8–12 September 1980; Alexander, J.M., Ed.; pp. 183–190.
30. Fais, A. Processing characteristics and parameters in capacitor discharge sintering. *J. Mater. Process. Technol.* **2010**, *210*, 2223–2230. [[CrossRef](#)]
31. Grigoryev, E.G.; Olevsky, E.A. Multiscale thermal processes in high voltage consolidation of powders. In *Processing and Properties of Advanced Ceramics and Composites V. Ceramic Transactions Volume 240*; Bansal, N.P., Singh, J.P., Ko, S.W., Castro, R.H.R., Pickrell, G., Manjooran, N.J., Nair, K.M., Singh, G., Eds.; John Wiley & Sons Inc.: Hoboken, NJ, USA, 2013; pp. 189–195.
32. Tagashira, K.; Ishihara, K.; Shingu, H.P. The consolidation of mechanically ground iron powders by electro discharge compaction. *J. Jpn. Soc. Powder Metall.* **1993**, *40*, 967–970. [[CrossRef](#)]
33. Alp, T.; Darvizeh, A.F.; Al-Hassani, S.T.S. Preforming of metal—Polymer composites by electrical discharge compaction of powders. *Powder Metall.* **1988**, *31*, 173–177. [[CrossRef](#)]
34. Al-Hassani, S.T.S.; Can, M.; Watson, E.J. A second order approximation to nonlinear circuit equations as applied to high energy electrical discharge processes. *J. Comput. Appl. Math.* **1986**, *15*, 175–189. [[CrossRef](#)]
35. Can, M.; Etemoglu, A.B. Porosity measurement of stainless steel filters produced by electrical discharge technique. *Filtr. Sep.* **2004**, *41*, 37–40. [[CrossRef](#)]
36. Schütte, P.; Garcia, J.; Theisen, W. Electro discharge sintering as a process for rapid compaction in PM-technology. In Proceedings of the International Powder Metallurgy Congress and Exhibition, Euro PM 2009, Copenhagen, Denmark, 12–14 October 2009; Volume 3, pp. 91–96.
37. Fais, A.; Actis Grande, M.; Forno, I. Influence of processing parameters on the mechanical properties of Electro-Sinter-Forged iron based powders. *Mater. Des.* **2016**, *93*, 458–466. [[CrossRef](#)]
38. Bogachev, I.; Yudin, A.; Grigoryev, E.; Chernov, I.; Staltsov, M.; Khasanov, O.; Olevsky, E. Microstructure investigation of 13Cr-2Mo ODS steel components obtained by high voltage electric discharge compaction technique. *Materials* **2015**, *8*, 7342–7353. [[CrossRef](#)] [[PubMed](#)]
39. Xiang, S.; Zhang, X. Residual stress removal under pulsed electric current. *Acta Metall. Sin. (Engl. Lett.)* **2020**, *33*, 281–289. [[CrossRef](#)]
40. Alitavoli, M.; Darvizeh, A. High rate electrical discharge compaction of powders under controlled oxidation. *J. Mater. Process. Technol.* **2009**, *209*, 3542–3549. [[CrossRef](#)]
41. Mohr, A.; Röttger, A.; Windmann, M.; Theisen, W. Rezyklieren von metallischen spänen mittels electro-discharge sintering. *Mater. Wiss. Werkst.* **2014**, *45*, 552–560. [[CrossRef](#)]
42. Egan, D.; Melody, S. EDS as a Method of Manufacturing Diamond Tools. *Met. Powder Rep.* **2009**, *64*, 10–13. [[CrossRef](#)]
43. Sizonenko, O.N.; Baglyuk, G.A.; Raichenko, A.I.; Bogatyreva, G.P.; Oleinik, N.A.; Taftai, É.I.; Lipyan, E.V.; Torpakov, A.S. Effect of high-voltage discharge on the particle size of hard alloy powders. *Powder Metall. Met. Ceram.* **2011**, *49*, 630–636. [[CrossRef](#)]
44. Sizonenko, O.N.; Baglyuk, G.A.; Raichenko, A.I.; Taftai, É.I.; Lipyan, E.V.; Zaichenko, A.D.; Torpakov, A.S.; Guseva, E.V. Theory, manufacturing technology, and properties of powders and fibers variation in the particle size of Fe–Ti–B4C powders induced by high-voltage electrical discharge. *Powder Metall. Met. Ceram.* **2012**, *51*, 129–136. [[CrossRef](#)]
45. Saida, J.; Tanaka, Y.; Tanaka, Y. Joining of Fe-Base amorphous alloy ribbons using high voltage discharging. *J. Jpn. Inst. Metals* **1998**, *62*, 607–616. [[CrossRef](#)]
46. Scardi, P.; D’inciau, M.; Leoni, M.; Fais, A. Dislocation Configurations in Nanocrystalline FeMo Sintered Components. *Metall. Mater. Trans. A* **2010**, *41*, 1196–1201. [[CrossRef](#)]
47. Fais, A.; Maizza, G. Densification of AISI M2 high speed steel by means of capacitor discharge sintering (CDS). *J. Mater. Process. Technol.* **2008**, *202*, 70–75. [[CrossRef](#)]
48. Nishikawa, W. The principle and application field of stud welding. *Weld. Int.* **2003**, *17*, 699–705. [[CrossRef](#)]

49. MPIF Standard 46; Determination of Tap Density of Metal Powders. In *Standard Test Methods for Metal Powders and Powder Metallurgy Products*. MPIF, Metal Powder Industries Federation: Princeton, NJ, USA, 2016.
50. Ugarteche, C.V.; Furlan, K.P.; Pereira, R.V.; Tringade, G.; Binder, R.; Binder, C.; Klein, A.N. Effect of microstructure on the thermal properties of sintered iron-copper composites. *Mater. Res.* **2015**, *18*, 1176–1182. [[CrossRef](#)]
51. Bardhan, P.K.; Patra, S.; Sutradhar, G. Analysis of density of sintered iron powder component using the response surface method. *Mater. Sci. Appl.* **2010**, *1*, 152–157. [[CrossRef](#)]
52. MPIF Standard 42; Method for Determination of Density of Compacted or Sintered Powder Metallurgy (PM) Products Materials. In *Standard Test Methods for Metal Powders and Powder Metallurgy Products*. MPIF, Metal Powder Industries Federation: Princeton, NJ, USA, 2022.
53. ISO Standard ISO 6507-1: 2018; Metallic Materials—Vickers Hardness Test—Part 1: Test Method. International Organization for Standardization: Vernier, Switzerland; Geneva, Switzerland, 2018.
54. Uhler, A.J. The potentials of infinite systems of sources and numerical solutions of problems in semiconductor engineering. *Bell Syst. Tech. J.* **1955**, *34*, 105–128. [[CrossRef](#)]
55. ASM Handbook. *Powder Metallurgy*; Samal, P., Newkirk, J., Eds.; ASM International: Materials Park, OH, USA, 2015; Volume 7.
56. Montes, J.M.; Cuevas, F.G.; Cintas, J.; Urban, P. A One-Dimensional Model of the Electrical Resistance Sintering. *Process. Metall. Mater. Trans. A* **2015**, *46*, 963–980. [[CrossRef](#)]
57. Sovizi, S.; Seraji, M.E. The densification behavior of metals and alloys during spark plasma sintering: A mini-review. *Sci. Sinter.* **2019**, *51*, 1–18. [[CrossRef](#)]
58. Cho, J.Y.; Song, G.A.; Choi, H.S.; Kim, Y.H.; Kim, T.S.; Lee, M.H.; Lee, H.S.; Kim, H.J.; Lee, J.K.; Fleury, E.; et al. Necking mechanisms on porous metallic glass and W compacts using electro-discharge sintering. *J. Alloys Comp.* **2012**, *536S*, S78–S82. [[CrossRef](#)]